International Research Journal of Environment Sciences ISSN 2319–1414
Vol. **2(10),** 77-92, October **(2013)** *Int. Res. J. Environment Sci.*

Carbon Dioxide driven Solar-assisted Heat Pump Water Heating System: A Theoretical Analysis

M. Raisul Islam and K. Sumathy
Department of Mechanical Engineering, North Dakota State University, Fargo, ND 58108, USA

Available online at: www.isca.in, www.isca.me
Received 15th September 2013, revised 25th September 2013, accepted 11th October 2013

Abstract

Details of the analytical studies of a CO_2 transcritical cycle on a solar assisted heat pump water heating system is presented in this paper. The main components of this system include an evacuated tube U-pipe solar collector serving as the evaporator for the R744 (CO_2) refrigerant, a variable speed reciprocating compressor, an immersed heat exchanger and an expansion valve. In general, solar heat pumps are known to provide higher values of COP since solar radiation can easily effect higher evaporation temperatures. However, incompatible weather conditions may affect the performance of heat pump, and hence an optimization of such system is essential which is dictated by the dominant operating parameters, such as: solar radiation, solar collector area, speed of the compressor, evaporating and condensing temperatures. A numerical model has been developed to optimize the system design and operating parameters. The developed simulation model can predict the performance of the system COP, solar collector efficiency and heat capacity. For the North Dakota USA weather conditions, the average COP range from 2-3 with solar collector efficiencies of about 40%-60% and temperature of the storage tank water range between 30º-45ºC.

Keywords: Solar water heating, heat pumps, CO_2, Refrigerant, COP.

Introduction

Rapid economic growth around the world is largely dependent on the excessive utilization of the fossil fuels (e.g. crude oil, coal etc.). In this process, large quantities of pollutants are being pumped into the atmosphere causing serious damage to the natural balance of the eco-systems. In addition to that, continual decrease of fuel deposition of the world compels intensive research in further developing the existing renewable energy resources. Since the signing of Kyoto protocol[1] to reduce greenhouse gas emissions by about 5%, the technologically developed countries have had a motivation to switch-over to the ecologically safe chlorine-free refrigerants.

The use of hydro-fluorocarbon (HFC) fluids was once thought to be the most acceptable replacement of hydro-chlorofluorocarbon (HCFC) fluids. However, both the categories are in the list of scheduled phase-out for their influence on environmental changes and as such their global warming potential (GWP) is far more high, typically above 150 GWP compared to CO_2. Hence, the growing concern over the use of such refrigerants renewed the interest in utilizing environmentally benign natural fluids, such as: water, air, ammonia, silicon oil, propane and CO_2. Among these fluids, water has freezing issues, when exposed to the weather conditions below 0°C. Similarly, the thermodynamic cycle dealing with air as working fluid has relatively low cycle efficiency. Ammonia also has its own drawback being slightly toxic. The use of silicon oil is restricted to its use due to the high viscosity. Although purified propane as refrigerant is gaining favor, but when mixed with air it is highly flammable. Concerning all these issues, CO_2 has a strong potentiality to be used as an alternative refrigerant as it is non-toxic, non-flammable, having very low GWP and neutral effect on depleting ozone layer. Moreover, its' inert gaseous behavior, readily availability overcomes the issues pertaining to the corrosion problems and production ability/distribution logistics.

The use of solar assisted heat pump (SAHP) increased as the commercial solar collectors entered into the market. Several researchers have developed and tested various SAHP models[2-5]. Conventional SAHP systems utilized the solar collector and heat pump as separate units and used an intermediate heat exchanger to complete the heat transfer circuit. However, recently developed direct-expansion solar assisted heat pump (DX-SAHP) systems integrate the solar collector and heat pump evaporator unit into a single unit[6-11]. The above mentioned types have used flat-plate solar collector as evaporator and halocarbons as refrigerant. A number of studies have also been performed to improve the existing solar collectors design as well as its efficiency[12-16]. The improvement methods include structural changes, introduction of new materials and coatings, and various working fluids.

Recently, one of the new collectors, namely, evacuated tube U-pipe solar collector has been studied recently in applications for electric power and heat generation using CO_2 as the working fluid[17-20]. Zhang and Yamaguchi[21] have studied the convective heat transfer characteristics of supercritical CO_2 in a horizontal circular tube in forced convection mode and identified several heat enhancement mechanisms which are superior to a water-

based collector system. In order to investigate the influence of CO_2 as a working fluid in a U-tube inserted glass evacuated solar collector, Zhang et al.[22] made a detailed study on the collector characteristics with CO_2 as the working fluid and found that the annually-averaged efficiency could attain above 60% which is much higher than the water-based collectors where annual maximum efficiency could reach only up to 50%. Earlier, the use of CO_2 was limited to mainly in marine refrigeration systems because of its lower critical point (7.38 MPa, 31.1°C). However, due to environmental concerns, renewed interests are shown towards CO_2 as the working fluid, because of its favorable heat transfer and thermodynamic properties. Moreover, CO_2 has high volumetric refrigeration capacity which makes the system design compact in nature[23].

In this paper, the use of CO_2 in a transcritical cycle has primarily been focused in which heat rejection occurs in the supercritical stage where only sensible cooling or heating takes place. The first CO_2 based transcritical cycle was introduced by Lorentzen[24] in 1990. Later on, several researchers conducted studies on transcritical CO_2 heat pump cycle for automotive cooling and heating applications[25-27]. Transcritical CO_2 cycle can also be applicable for water heating purposes where large temperature increments are generally required. Literature shows that there exist several studies on transcritical CO_2 heat pump water heaters[28-34]. A detailed comparative study[33] between heat pump water heater using CO_2 and R134 a has been presented by Cecchinato et al. and concluded that CO_2 could be a potential alternative for synthetic refrigerants. Richter et al[35] reported that when a heat output is subjected to low outdoor temperatures CO_2-based heat pump water heating system showed higher heating capacity than a similar system using R410a.

A computer simulation model for DX-SAHP system (water heating purposes) using CO_2 in a transcritical cycle, has been developed and is presented in this paper. The current study also aims at using evacuated tube U-pipe solar collector as evaporator and examines the parametric performances. Several operating parameters, such as: solar radiation, collector area, compressor speed and storage volume are varied to obtain the optimal performances of the system in terms of COP, collector efficiency and heating capacity. The results will be useful for designing and optimizing such type of DX-SAHP system using CO_2 as refrigerant.

System description and thermodynamic cycle: DX-SAHP water heating system consists of an evacuated tube U-pipe solar collector as an evaporator, a compressor, an immersed heat exchanger in a hot water storage tank which acts as a condenser and an expansion device (figure 1).

The system investigated in this paper is studied for water heating applications by the use of CO_2 in the transcritical thermodynamic cycle and uses the meteorological data in the fall, winter and spring conditions of Fargo, North Dakota, USA. Initially, CO_2 passes directly through the heat removal U-pipe that is inserted into the evacuated tube solar collector where it gets heated and eventually evaporated by the incident solar radiation. Depending on the operating conditions in the evaporator, the atmospheric air acts like an additional heat source or sink. The thermodynamic process undergone by CO_2 is shown in the idealized pressure-enthalpy diagram (figure 2). The path 4-1 represents the evaporation process in which CO_2 undergoes phase change from liquid to vapor. The evaporated refrigerant is then compressed in the subsequent compression process 1-2 to a supercritical vapor pressure stage. The supercritical CO_2 at a high pressure and temperature goes through the process 2-3 in the condenser, where the working fluid gets condensed. The energy released by the supercritical CO_2 vapor (in coil condenser) is then utilized to heat the water by sensible cooling process through a heat exchanger, which has been immersed into the hot water storage tank. Finally, the high pressure but low temperature CO_2 is throttled to the evaporator pressure by the throttling process shown as process 3-4, where pressurized CO_2 flashes through the thermostatic expansion valve to attain its initial pressure conditions (evaporator pressure). This completes one full cycle. Subsequent cycles follow the same sets of events, by which water in the storage tank eventually gets heated up. The process continues as long as solar radiation is available on the solar collector. As shown in figure 2, the transcritical cycle shares a low-pressure sub-critical zone and a supercritical high pressure side in any given cycle of operation. In the studied transcritical cycle, it is ensured that CO_2 is compressed close to its critical point. This is because, one of the distinct characteristics of supercritical CO_2 is that, near the critical point it shows a rapid change in thermodynamic and transport properties even with a small change in temperature. This particular region is called the 'pseudo-critical' zone where the specific heat coefficient reaches the maximum for a given pressure and temperature[28].

Modeling and simulation procedure: The mathematical modeling of the proposed DX-SAHP system to predict the thermodynamic performance is simplified based on the following general assumptions: i. Quasi-steady state conditions are approximated within the chosen time interval. ii. The refrigerant is uniformly distributed among all the heat removal pipes in the evacuated tube solar collector and is considered to be saturated at the exit of the collector. iii. Pressure drop and heat loss in the connecting pipes are neglected. iv. Frictional losses in the evaporator and the condenser are negligible. v. A good thermal insulation over the CO_2 loop is assumed, i.e. thermal loss to the surroundings is neglected. vi. A non-stratified hot water storage tank is considered for the simulation. vii. Kinetic and potential energy changes are assumed to be insignificant. The overall DX-SAHP water heating system consists of four individual process-models and each of the processes corresponds to the individual component of the model. In order to predict the thermal performance of the total system, each component is analyzed theoretically. The above assumptions are made to formulate the governing equations of each component of the system which will be described in the following sections.

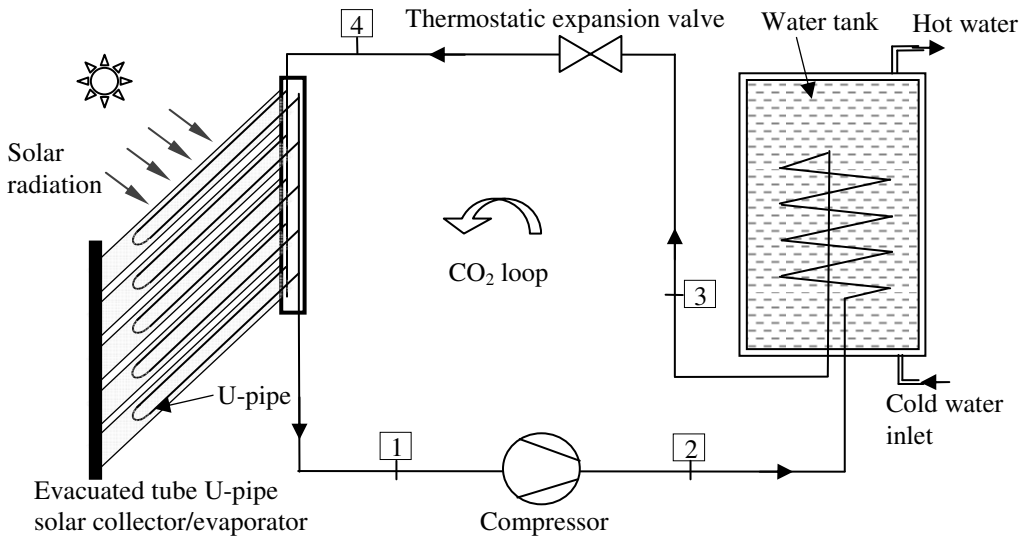

Figure-1
Schematic diagram of a direct-expansion solar assisted heat pump water heating system

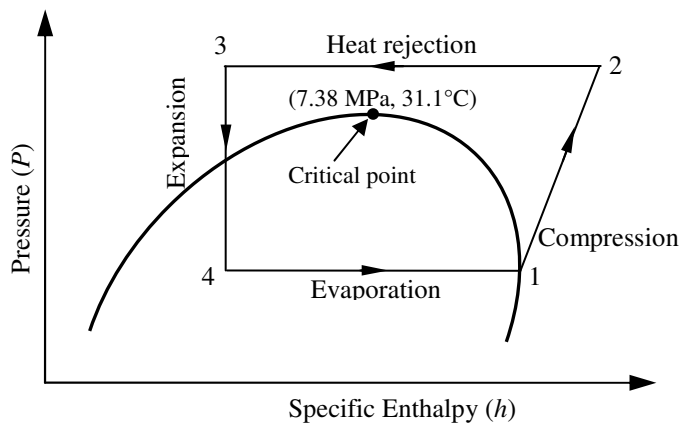

Figure-2
P-*h* diagram of transcritical CO_2 heat pump cycle

Evaporator model: The evaporator component (U-pipe inserted glass evacuated tube solar collector) of the heat pump system used in this study is shown in figure 3. Important features of this system are: (a) the outer and inner glass tubes placed concentrically to provide the vacuum space in between them, (b) selective absorber coating painted inside the inner tube and (c) copper U-pipe placed inside the inner glass tube with a fin connected together. The characteristic features of glass evacuated tube solar collectors are its collective effect of vacuum insulation between the concentric tubes and the selective surface coatings that results in enhanced heat extraction efficiency, which is far more superior to that of a flat-plate solar collector[15]. As the solar radiation passes through the glass tubes, it is absorbed by the surface coating placed inside the inner tube. The absorbed heat is then transferred to the U-tube by conduction and in then to the working fluid inside the U-tube by convection heat transfer method effecting an increase in the temperature and pressure of the working fluid.

Following assumptions are made to simplify the one-dimensional heat transfer analysis of the evacuated tube U-pipe solar collector used in the present study: i. Heat absorption by the outer glass tube of the solar collector is considered insignificant. ii. Thermal resistances of the outer glass tube, surface coating, metal tube and fin are neglected. iii. Radial temperature gradients among surface coating, metal U-tube and fin are assumed to be negligible. iv. Averaged heat flux in the circumferential direction is used as the boundary condition[16].

The useful heat gain (Q_u) of the solar collector is defined as

$$Q_u = A_{coll} F' \left[I_T \left(\tau_g \alpha_g \right) - U_L \left(T_f - T_a \right) \right] \quad (1)$$

In equation 1, overall heat loss coefficient (U_L) is defined as the sum of top loss coefficient (U_t) and edge loss coefficient (U_e).

$$U_L = U_t + U_e \tag{2}$$

Edge loss coefficient is neglected due to the assumption of proper heat insulation at the edges of the solar collector. Top loss coefficient (U_t) can be defined as:

$$U_t = \left(\frac{1}{h_{g,conv}} + \frac{1}{h_{g,r}} + \frac{1}{h_{g,cond}} \right)^{-1} \tag{3}$$

where $h_{g,conv}$ is the heat transfer coefficient between the outer glass tube and the ambient due to convection (W m^{-2} K^{-1}), $h_{g,r}$ is the radiation heat transfer coefficient from the inner glass tube to the outer glass tube (W m^{-2} K^{-1}) and $h_{g,cond}$ represents conduction heat transfer coefficient between the inner glass tube and the fin (W m^{-2} K^{-1}). The heat transfer coefficient $h_{g,conv}$ and $h_{g,r}$ can be written as:

$$h_{g,conv} = 5.7 + 3.8V \tag{4}$$

$$h_{g,r} = \frac{\sigma \varepsilon_{at}}{1 + \frac{\varepsilon_{at} D_{at}}{\varepsilon_g D_g}(1 - \varepsilon_{at})} \left(T_{at}^2 + T_g^2\right)\left(T_{at} + T_g\right) \tag{5}$$

The conduction heat transfer coefficient expressed in equation (3) and the edge loss coefficient can be obtained from the theoretical[16] and experimental results[36] which were calculated as 0.2796 (W m^{-2} K^{-1}) and 0.1687 (W m^{-2} K^{-1}) respectively. From the Figure 3(c), the heat loss of the evacuated tube can be written as:

$$U_t\left(T_{at} - T_a\right) = h_{g,r}\left(T_{at} - T_g\right) + h_{g,cond}\left(T_{at} - T_g\right) \tag{6}$$

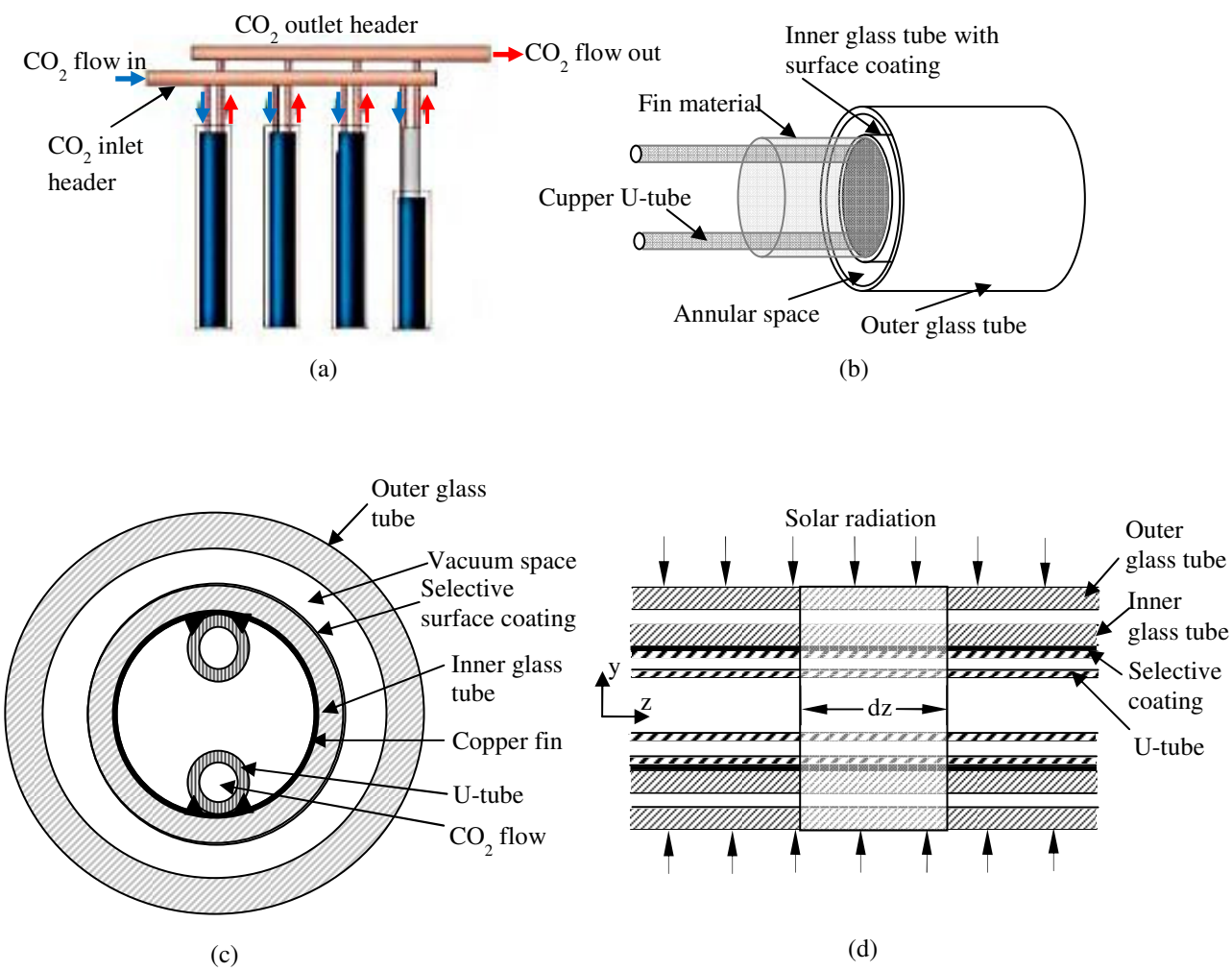

Figure-3
Flow direction of the working fluid inside the evacuated tube U-pipe solar collector and its components. (a) CO_2 flow direction; (b) construction of the unit glass tube; (c) cross-sectional view of the collector tube; and (d) differential control volume used in the present analysis

In the above equations (3)-(6), the unknown parameters are U_t, $h_{g,r}$, V, T_{at}, T_g and T_a. Using the known parameters V, T_{at} and T_a rest of the unknown parameters have been calculated by iterative numerical procedure (secant method). The calculated values are then used to compute the overall heat loss coefficient of the solar collector which is one of the important parameters to estimate the performance of the solar collector.

The collector efficiency factor (F') is determined by the following formula as given by Hottel-Whilliar Bliss model[4].

$$F' = \frac{1/U_L}{W\left[\frac{1+U_L/C_b}{U_L[d+(W-d)F]} + \frac{1}{C_b} + \frac{1}{h'_f \pi d}\right]} \tag{7}$$

The standard fin efficiency (F) is given as:

$$F = \frac{\tanh[m(W-d)/2]}{m(W-d)/2} \tag{8}$$

and the constant value, m is defined as:

$$m = \left[\frac{U_L}{\lambda\delta(1+U_L/C_b)}\right]^{1/2} \tag{9}$$

For the evaluation of inner tube temperature (T_{at}), copper tube connected between the inlet and outlet of metal U-tubes is treated as fin and a second-order temperature equation is derived by considering a small element on the fin[16].

$$\frac{d^2T_{at}}{dy^2} = \frac{-S + U_L(T_{at}-T_a)}{\lambda\delta(1+U_L/C_b)} \tag{10}$$

Temperature of the working fluid inside the U-tube is determined by dividing the evaporation process into differential control volumes of length dz shown in figure 3(d). Such discretization is employed to improve the accuracy of the calculation and the thermo-physical property variations near the critical region of the CO_2. Thermodynamic properties are assumed to be constant in each of the differential control volume segments. The calculated outlet properties of each element then become the inlet state of the successive element. Applying the first law of thermodynamics to each segment of the differential elements, the following thermal expressions are obtained.

Outer glass tube:

$$\alpha_g r_g I_T + r_{at} h_{at}(T_{at}-T_g) + \frac{r_{at}\sigma(T_{at}^4 - T_g^4)}{1/\varepsilon_g + (r_{at}/r_g)(1/\varepsilon_g - 1)} = r_g h_a (T_g - T_a) + r_g \sigma \varepsilon_g (T_g^4 - T_a^4) \tag{11}$$

Inner glass tube:

$$\tau_g \alpha_g r_{at} I_T + \frac{K_g(T_c - T_{at})}{\ln\left[1+\left(\frac{\delta_{at}}{2r_{at}}\right)\right]} = r_{at} h_{at}(T_{at}-T_g) + \frac{r_{at}\sigma(T_{at}^4 - T_g^4)}{1/\varepsilon_g + (r_{at}/r_g)(1/\varepsilon_g - 1)} \tag{12}$$

Surface coating and U- tube:

$$\tau_g^2 \alpha_c r_{at} I_T = \frac{K_g(T_c - T_{at})}{\ln\left[1+\left(\frac{\delta_{at}}{2r_{at}}\right)\right]} + 2r_m h_c (T_c - T_f) \tag{13}$$

Working fluid (CO_2):

$$m_f C_P \frac{dT_f}{dz} = r_m h_c (T_c - T_f) \tag{14}$$

The equation 11 through equation 14 are further simplified to formulate as a single expression in first order differential equation, to calculate the temperature of the working fluid.

$$\frac{dT_f}{dz} = \frac{\tau_g^2 \alpha_c r_{at} I_T + \tau_g \alpha_g r_{at} I_T + \alpha_g r_g I_T - r_g \sigma \varepsilon_g (T_g^4 - T_a^4) - r_g h_a (T_g - T_a)}{2 m_f C_P} \tag{15}$$

The heat transfer coefficient (h'_f) of the working fluid for the two-phase flow region in the horizontal tubes is defined by the following relationship[37].

$$h'_f = \frac{0.0082 K_f}{d_i}\left(\mathrm{Re}_{d_i}^2 \, J \Delta x h_{fg}/L\right)^{0.4} \tag{16}$$

where J is the dimensional constant with a fixed value of 778 and Δx is the change in quality of the CO_2 between inlet and exit state[37]. Quality change in the above equation is assumed due to the enthalpy change only, neglecting the pressure effects on the quality. Reynolds number is based on internal diameter (d_i) and liquid viscosity of the two-phase CO_2. In the superheated region, the h'_f is obtained using the following Dittus-Boelter relationship.

$$h'_f = 0.023 \mathrm{Re}_{d_i}^{0.8} \mathrm{Pr}_{d_i}^{0.4} \frac{K_f}{d_i} \tag{17}$$

Pressure drop of CO_2 inside the U-tube is obtained by considering the homogeneous two-phase mixture flow and by using mass, momentum, and energy balance relationship explained by Chaturvedi et al.[37]. The simplified correlations are listed below.

$$\frac{dP}{dz} = -\frac{\frac{2C_f G^2}{d_i}\left(v_f + xv_{fg}\right) + G^2 v_{fg}\frac{dx}{dz}}{\left(1 + G^2\left(x\frac{dv_g}{dP} + (1-x)\frac{dv_f}{dP}\right)\right)} \quad (18)$$

$$\dot{m}_f \frac{dx}{dz} = \frac{WF'}{h_{fg}}\left[I_T(\tau\alpha) - U_L\left(T_f - T_a\right)\right] \quad (19)$$

The frictional pressure drop coefficient (C_f) depends on the laminar and turbulent nature of the fluid flow inside the U-tube which is the function of Reynolds number and it is defined using the following:

$$C_f = \frac{16}{\mathrm{Re}_{d_i}}, \mathrm{Re} < 2300 \quad (20)$$

$$C_f = \frac{0.079}{\mathrm{Re}_{d_i}^{0.25}}, \ \mathrm{Re} \geq 2300 \quad (21)$$

In equation (18), the saturated fluid properties are calculated by choosing a polynomial fit curve for v_f, v_g and v_{fg} as a function of pressure. A fourth-degree polynomial fit is chosen to find the above properties of CO_2 which is valid in the pressure range of 2-7.3 MPa. The error involved by this polynomial fit remains within 1% range and is mainly useful for numerical solution method. The degree of superheating in each iterative process is evaluated using the following expression.

$$\Delta T = T_1 - T_1' \quad (22)$$

The superheated single-phase region starts at the length of U-tube denoted as z_0 and can be written as

$$z_0 = -\frac{C_{pv}\log_e\left[\frac{T_1 - T_a - S/U_L}{T_1' - T_a - S/U_L}\right]\dot{m}_f}{F'U_L W} \quad (23)$$

The instantaneous efficiency of the solar collector is given as:

$$\eta_{coll} = \frac{Q_u}{A_{coll} I_T} \quad (24)$$

The useful energy received by the solar collector can also be obtained as a function of the change in enthalpy of the inlet and outlet (exit) state of the collector.

$$Q_e = \dot{m}_f \Delta h \quad (25)$$

Compressor model: The mass flow rate of the carbon dioxide through the compression process is obtained by the following expression as:

$$\dot{m}_f = \rho_{suc}\eta_v V_s \frac{N}{60} \quad (26)$$

where N is denoted as compressor speed in rpm. The swept volume (V_s) is estimated using the following formula.

$$V_s = i\frac{\pi D_b^2 S}{4} \quad (27)$$

The volumetric (η_v), mechanical (η_m) and isentropic (η_{isen}) efficiency formulas of the compressor is used from the correlations developed by Oritz et al.[38]. All the efficiency expressions are obtained as the function of suction to discharge pressure ratios.

$$\eta_v = \frac{\dot{m}_f}{\rho_{suc}V_s N/60} = 0.9207 - 0.0756\left(\frac{P_{dis}}{P_{suc}}\right) + 0.0018\left(\frac{P_{dis}}{P_{suc}}\right)^2 \quad (28)$$

$$\eta_m = \frac{W_{com}}{P_i} = 0.9083 - 0.0884\left(\frac{P_{dis}}{P_{suc}}\right) + 0.0051\left(\frac{P_{dis}}{P_{suc}}\right)^2 \quad (29)$$

$$\eta_{isen} = \frac{h_{2,isen} - h_1}{h_2 - h_1} = -0.26 + 0.8952\left(\frac{P_{dis}}{P_{suc}}\right) - 0.2803\left(\frac{P_{dis}}{P_{suc}}\right)^2 + 0.0414\left(\frac{P_{dis}}{P_{suc}}\right)^3 - 0.0022\left(\frac{P_{dis}}{P_{suc}}\right)^4 \quad (30)$$

The internal compression work (W_{com}) is the function of power consumption which depends on the mass flow rate, isentropic efficiency and the isentropic enthalpy change of the refrigerant.

$$W_{com} = \dot{m}_f \frac{\left(h_{2,isen} - h_1\right)}{\eta_{isen}} \quad (31)$$

Compressor work can also be expressed in terms of enthalpy change of refrigerant between the inlet and outlet state.

$$W_{com} = \dot{m}_f\left(h_2 - h_1\right) \quad (32)$$

Condenser/hot water storage tank model: For the water storage tank model, water temperature within the tank is assumed to be uniform at any instance of time. The schematic and the modes of heat transfer between CO_2 and water in the storage tank is shown in detail in Figure 4. The hot water demand is supplied to the load directly from this tank. Therefore, for non-stratified or a mix tank model with the immersed condenser, the following expression could be used to evaluate the increment rise in water temperature.

$$M_w C_{pw}\frac{dT_w}{dt} = Q_{con} - (UA)_t\left(T_w - T_a\right) - Q_{load} \quad (33)$$

Heat rejected in the condenser to the water in the storage tank takes into account of the heat absorbed by the evaporator model and the work done by the compressor.

$$Q_{con} = Q_u + W_{com} \quad (34)$$

Similarly, the total heat dissipation from the condenser is also obtained by the following expression.

$$Q_{con} = (UA)_{coil}\left(T_{con} - T_w\right) \quad (35)$$

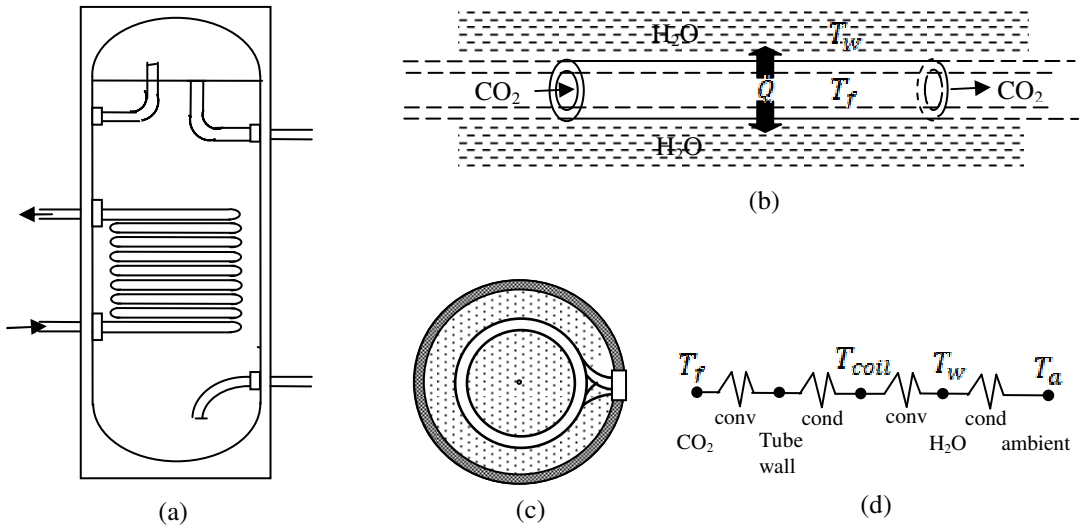

Figure-4
Hot water storage tank with immersed single coil condenser: (a) schematic of the storage tank; (b) heat transfer between CO_2 flow to the surrounding water; (c) top view of storage tank; and (d) thermal network between the CO_2 flow to the ambient

In the above expression (equation 35), $(UA)_{coil}$, is the overall heat transfer coefficient of the condenser coil. It is the sum of the thermal resistive values, including the convective resistance offered by CO_2, conductive resistance of the cooling coil and convective resistance of the water.

$$(UA)_{coil} = \left(\frac{1}{h_c' A_{c,i}} + \frac{\delta_{coil}}{K_{coil} A_{c,o}} + \frac{1}{h_w' A_{coil}} \right)^{-1} \quad (36)$$

The condensation process will be in the supercritical region for any steady-state cycle and hence it follows the single-phase sensible cooling process. The heat transfer coefficient of CO_2 within cooling coil to the inner tube wall of the cooling coil is evaluated using the following Nusselt correlation.

$$h_c' = \frac{K_c Nu_i}{d_i} \quad (37)$$

The overall Nusselt number (Nu_i) within the cooling coil includes the temperature drop across and is evaluated based on the Petukhov-Popov correlation[39].

$$Nu_i = \frac{(f/8)}{K_1 + K_2 (f/8)^{1/2} (\Pr^{2/3} - 1)} \quad (38)$$

where the friction factor f and the constants K_1 and K_2 are defined as:

$$f = (1.82 \ln(\mathrm{Re}) - 1.64)^{-2} ;\ 3000 \le \mathrm{Re} \le 5\times10^6 \quad (39)$$

$$K_1 = 1 + 3.4 f \quad (40)$$

$$K_2 = 11.7 + 1.8/(\Pr)^{1/3} \quad (41)$$

Similarly, the outside film coefficient between the outer tube walls to the water in the storage tank is evaluated using immersed heat exchanger tested by Farrington and Bingham[40].

$$h_0 = \frac{K_{wall} Nu}{d_0} \quad (42)$$

$$Nu = 0.9 Ra_{d_o}^{0.25} \quad (43)$$

The Rayleigh number in the Eq.(44) is defined as:

$$Ra_{d_o} = Gr_{d_o} \Pr = \frac{g\beta d_o^3 (T_{wall} - T_w)}{\upsilon^2} \cdot \frac{\mu C_P}{K_w} \quad (44)$$

Pressure drop of CO_2 through the immersed condenser is calculated using the Darcy friction factor, using the Blasius correlation for the flow in a smooth tube.

$$\Delta P = f \frac{\Delta L}{2\rho_c} \left(\frac{G_c^2}{d_i} \right) \quad (45)$$

Expansion device: The CO_2 pressure drop from condenser pressure to the evaporator pressure is effected through a thermostatic expansion valve. Ideally, the throttling process is assumed to be isenthalpic, and considered to be a steady state device.

The performance of the entire DX-SAHP system is predicted by evaluating the heating capacity and the coefficient of performance (COP). Heating capacity is the amount of heat rejected by the condenser (equation 35) and the COP reflects the

ratio of the heat rejection by the condenser (Q_{con}) to the electrical power required to operate the compressor (W_{com}).

$$COP = \frac{Q_{con}}{W_{com}} \quad (46)$$

Flow Chart of Simulation Program: A numerical computational model in MATLAB has been developed to analyze the characteristics of the above mentioned components, which holistically dictates the thermal performance of the DX-SAHP system. Input parameters (table 1) for the simulation cycle include: collector properties (table 1), meteorological data[41], initial storage water temperature and the compressor speed. The thermodynamic properties of the CO_2 used in analyzing each component of the system were generated using REFPROP 8.0 software.

Table-1
Main parameters used in the performance evaluation of DX-SAHP water heating system

Components	Parameters	Value
Evacuated tube U-pipe solar collector Properties of absorber coating	Absorbtance	0.927
	Transmittance	0.08
	Reflectance	0.033
Properties of glass tubes	Thermal conductivity	1.25 (W m^{-1} K^{-1})
	Transmittance	0.90
	Absorbtance	0.05
	Reflectance	0.05
	Emittance	0.83
	Outer tube outer diameter	47 mm
	Thickness	1.2 mm
	Inner tube outer diameter	37 mm
	Length of the tube	1.7 m
Properties of U-tube	Outer diameter	8 mm
	Conductivity	400 (W m^{-1} K^{-1})
	Bond conductance	30 (W m^{-1} K^{-1})
Compressor (Reciprocating-type, hermetic)	Swept volume per stroke	0.00001972 m^3
Condenser/ Storage tank	Thermal conductivity of insulation	0.0346 (W m^{-1} K^{-1})
	Thickness of insulation	5 mm
	Outer diameter of the condenser coil	8 mm
	Thickness	1 mm
Simulation parameters (standard)	Initial water temperature	7°C (winter) 15°C (fall and spring)
	Wind speed	3.5 (m s^{-1}) (all seasons)

Figure 5 describes the flow chart of the simulation procedure. To start a simulation cycle, the operating parameters are set as input, along with the assumed solar collector and condenser temperature at the outlet state. The collector temperature (T_{at}) is determined by adjusting the initial guessed degree of superheat value. The compressor and solar collector model are called upon to determine the inlet and outlet state of each process. Once the solar collector temperature has come under the specified tolerance limit, the program proceeds to evaluate the outlet state of the condenser. Finally, the condenser temperature is adjusted with the value less than the tolerance limit and the current operating condition is considered as steady-state. The program evaluates all the inlet and outlet states of each components of the system, heat gain of the collector, heating capacity, compressor power, and COP.

Results and Discussion

Theoretical analysis performed in section 3 is used here to show the thermal performance of the proposed DX-SAHP water heating system in terms of COP, solar collector efficiency and heating capacity. A number of operating parameters such as: solar radiation, collector area, compressor speed, ambient temperature and storage volume, strongly influence the overall performance of the system, and are used to investigate the system under study. The simulation model identifies the important variables and therefore enables to perform the parametric study. A standard case is defined to evaluate the effects of various parameters and is listed in table 1. To evaluate the effect of each parameter, all other variables remain constant at their standard values. The inlet water temperature to the storage tank is taken as an average of circulating tap water temperature.

Effect of compressor speed and collector area: To avoid the two-phase properties at the inlet of the compressor, it is assumed to deal with only the vapor phase discharged from the solar collector as either saturated vapor or at supercritical state. Therefore, though a part of the solar collector will go through the two-phase region, it is ensured that it is in the vapor region before entering into the compressor inlet. Throughout the steady state cycle shown in figure 2, it is observed from the simulated results that a transcritical operating condition is achieved. A heat sink of relatively low temperature (-5°C-10°C) plays a key role to ensure efficient transcritical operation.

The effect of compressor on the overall system performance is assessed by varying the speed of the compressor. Figure 6 shows the effect of compressor speed within a range of 900 to 1500 rpm on COP and heat output at the condenser, for different solar intensity levels. The collector area and the ambient temperature were set to the base values of 1.91 m^2 and 10°C, respectively. At any given speed of the compressor, COP increases with an increase in the solar intensity. It is due to the fact that solar intensity has a positive influence on the evaporation temperature, in turn requiring only low compressor speeds to accomplish the task of raising the fluid's temperature to the desired value. It could also be noted from the figure 6 that, as the compressor's speed increases, the COP value reduces. It is due to the fact that the discharge temperature

increases along with an increase in speed of the compressor. At lower compressor speeds (around 1000 to 1100 rpm), the DX-SAHP system could reach a COP value of 2-2.5 with a heat capacity rate of about 2.4-3.0 kW. However, as the speed of the compressor further increases, the COP value decreases, although the heat extraction rate is much higher. This is due to the fact that, increase in the compressor speed is aided only with the work input which reflects in lower COP values.

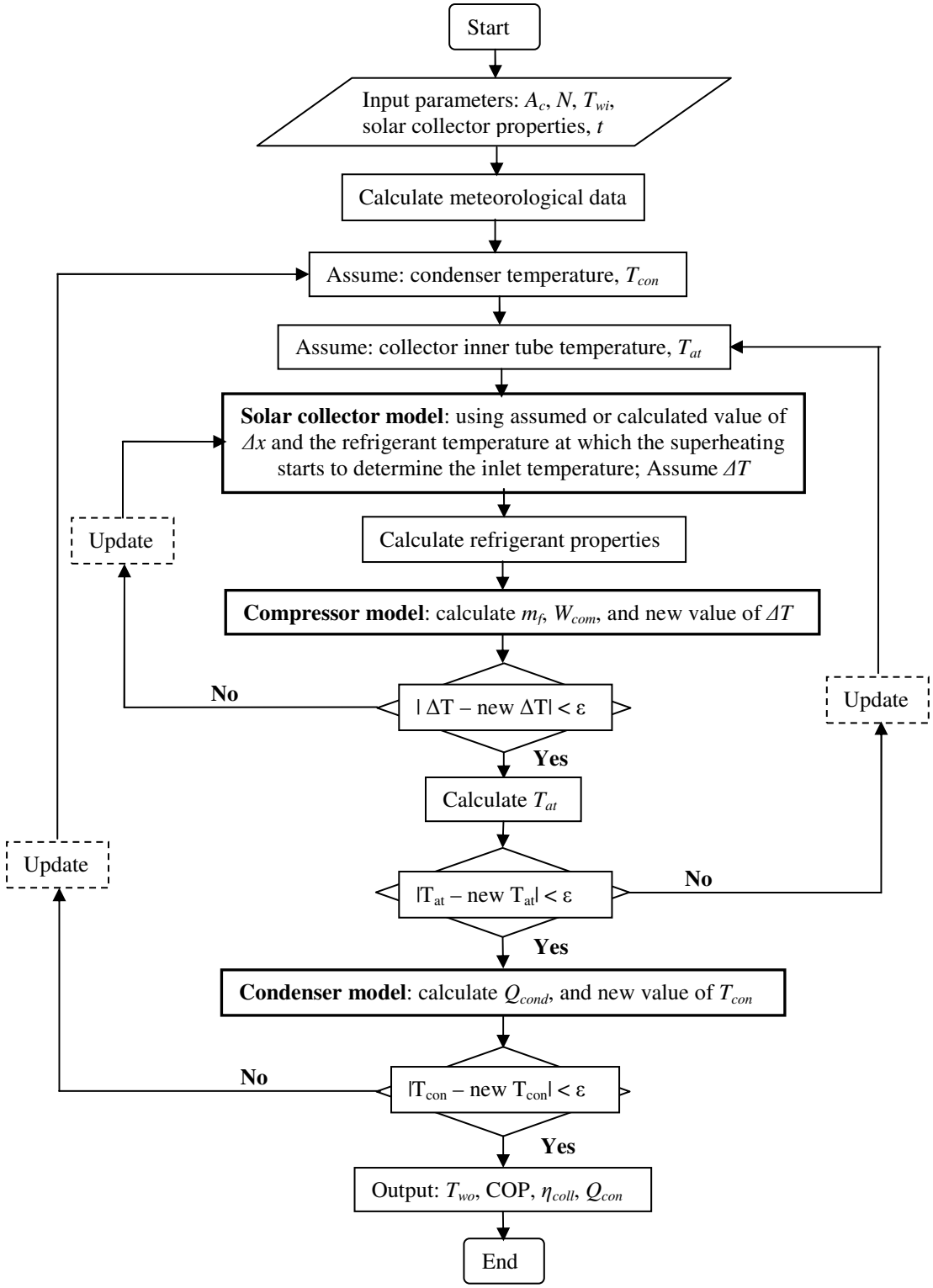

Figure-5
Flow chart of the simulation model

Figure 7 illustrates the variation of COP as a function of compressor speed considering solar collector area as a parameter. For a fixed compressor speed, the COP rises with the increase in collector area. If the solar collector area is more, the working fluid evaporates in the evaporator comparatively at a higher temperature which results in decrease in the compressor work and thus leading to a higher COP. Effect of the compressor speed on solar collector efficiency and evaporation temperature are shown in figure 8. The results have been predicted for the solar radiation of 600 W m^{-2} and collector area of 1.91 m^2. An increase in the compressor speed facilitates higher refrigerant mass flow rate through the solar collector which lowers working fluid temperature. This phenomena leads to a lower heat loss from the solar collector and increase the solar collector efficiency. However, for any given compressor speed, as the collector area increases, it effects higher working fluid temperature, eventually leading to a decrease in the collector efficiency. This performance disparity between the system COP and the solar collector efficiency, for the given collector size and ambient conditions, shows that, there is room to identify an optimum compressor speed, which will help in attaining a reasonable value in the COP and solar collector efficiency. Based on the results it could be discerned that, the predicted optimal compressor speed matches the existing collector design. In the situation of mismatches, it can be easily overcome by integrating a variable speed compressor to the DX-SAHP system, which would ensure an increase in the seasonal thermal performance.

Effect of ambient temperature and wind speed: Since the solar radiation intensity, ambient temperature and wind speed play a major role towards seasonal changes, the effect of these parameters on the system performance are analyzed and presented in this section. The effect of solar intensity has been depicted in figure 6, which shows its relative influence on the system performance. For a given solar intensity of 600 W m^{-2}, the influence of ambient temperature and wind speed variations are simulated and tabulated in table 2. It could be observed from the table 2 that higher ambient temperatures have a positive influence on the system in terms of both COP and collector efficiency. This is due to the fact that, the proposed system operates on heat-pump mode, and hence requires less work input towards compression. Similarly, for the given operating range, the collector efficiency is also shown to have an increase in the performance, because of the fact that collector heat losses are lower with increase in ambient temperature.

Wind speed also plays a pertinent role in the system performance. As one would expect, an increase in the wind speed would enhance the heat transfer between the solar collector and the surroundings. Under the conditions when the absorber tube temperature (T_{at}) is lower than the ambient temperature (T_a), an increase in the wind speed increases forced convection currents between the surrounding and absorber tube, resulting in higher rates of heat transfer. However, based on this study (table 2) with the given operating conditions, the effect of wind speed is not predominant compared to other operating parameters.

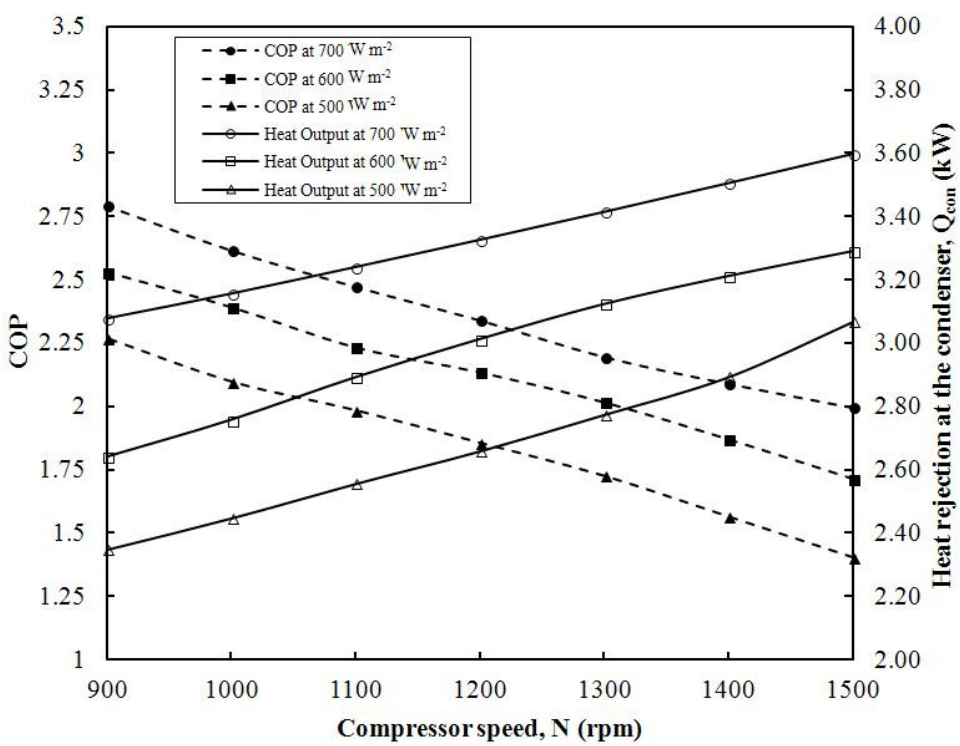

Figure-6
Effect of compressor speed on system COP and heat rejection at the condenser

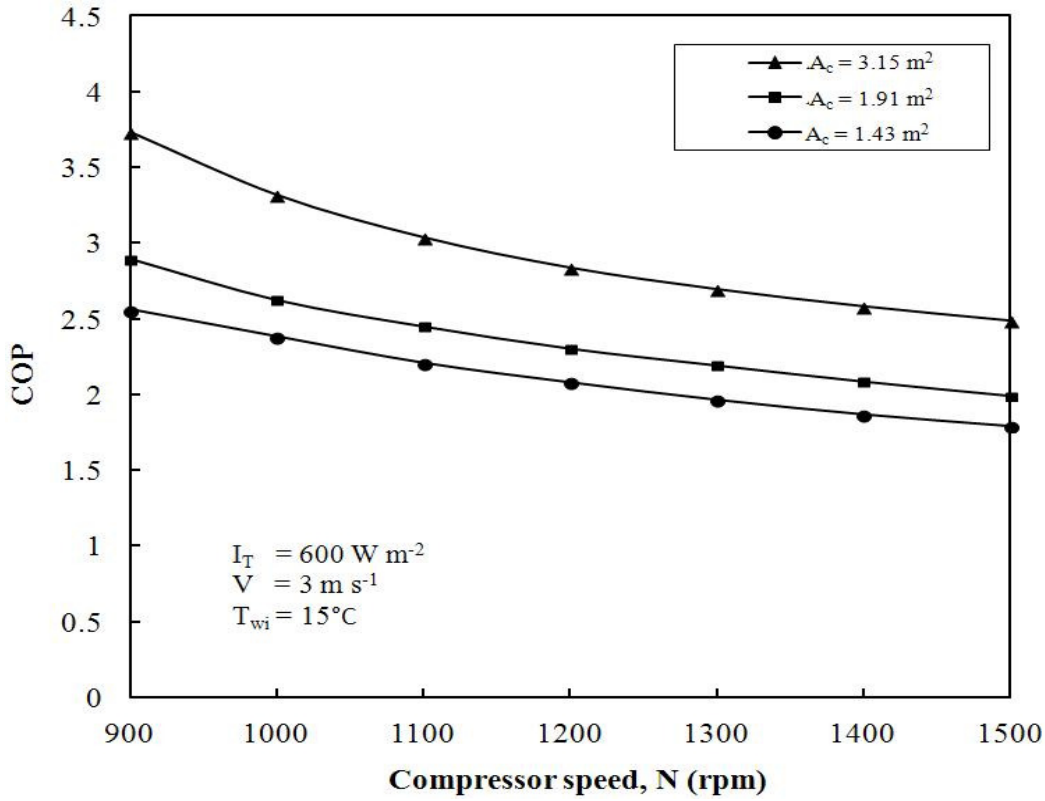

Figure-7
Effect of compressor speed for different collector area

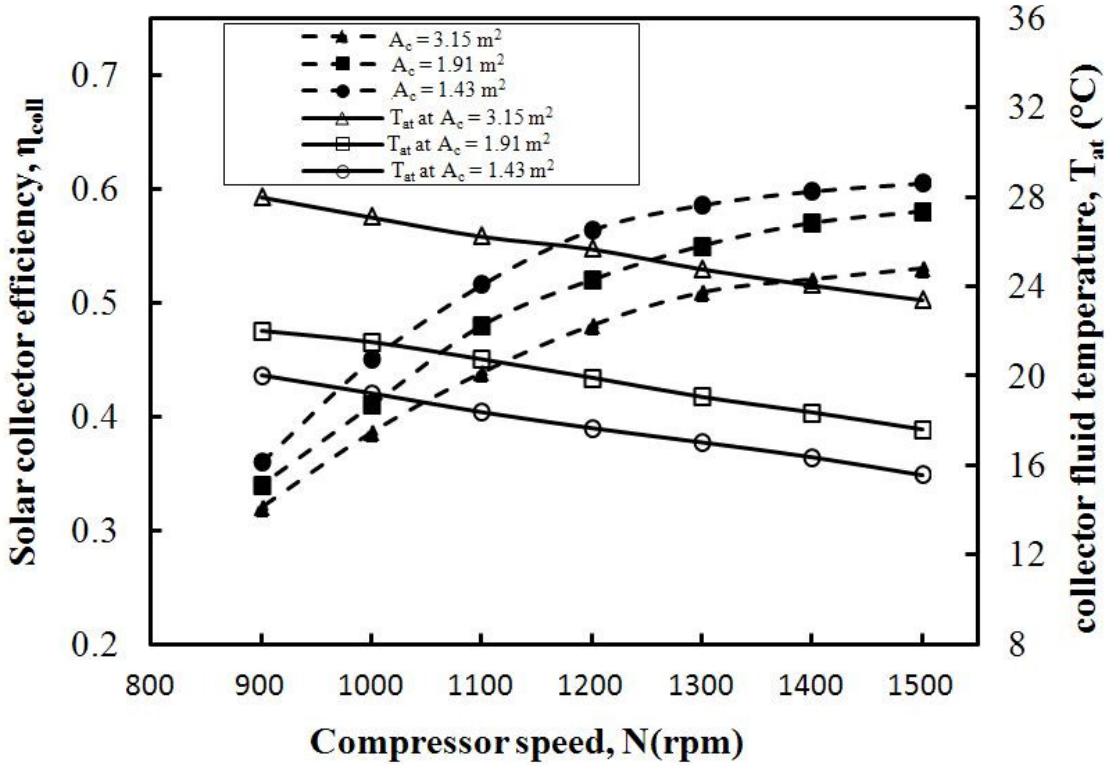

Figure-8
Variation of collector tube temperature and solar collector efficiency with compressor speed

Table-2
Effect of ambient temperature and wind speed on system performance

Weather parameters [a]		COP	Collector efficiency, η_{coll} (%)
Ambient Temperature, T_a (ºC)	-10	1.9637	33.05
	-5	2.0582	37.50
	0	2.1545	44.10
	5	2.2995	48.07
	10	2.4320	51.20
	15	2.6063	54.01
	20	2.7963	55.20
Wind Speed, V (m s^{-1})	1	2.6063	53.50
	2	2.6538	53.90
	3	2.7013	54.30
	4	2.7488	54.62
	5	2.7963	55.04

[a] Base values: I_T = 600 W m^{-2}, T_a = 10ºC, V = 3 m s^{-1}

Effect of condensing temperature: Condensing temperature (T_{con}) is also an important operating parameter that influences the system performance. For the given base-case figure 9(a) illustrates the effect of T_{con} on COP and collector efficiency and it could be seen that with an increase in T_{con}, though there is a sharp reduction in COP value, the collector efficiency reduces only marginally. Higher condenser temperature interprets that the collector absorber tube temperature is higher which aids higher heat losses from the collector system. Hence, the COP of the heat pump cycle, is dictated both by the T_{con} and T_{at}. A substantial rise in the condensing temperature along with a marginal increase in collector temperature leads to a considerable drop in the COP. Also, it could be apparent from figure 9(a) that, at low condensing temperature, both COP and collector efficiency are relatively higher. This observation suggests that the proposed heat pump cycle is more suitable for low temperature applications like domestic water heating. Similar to the condensing temperature, the evaporating temperature also plays a role on the overall system performance. Figure 9(b) shows that an increase in evaporating temperature improves the COP of the system positively. It should also be noted from figure 9 (a and b) that both condensing temperature and evaporating temperature have an inverse relationship on the COP of the system. Hence, for a given collector area of 1.91 m^2, it is better to operate the system with a storage water temperature (condensing temperature) within the range of 40°C - 45°C. Higher condensing temperature results in lower COP values, because of the fact that higher compression ratio (indicates the need for work input) is required to aid higher condensing temperature.

Combined effects of solar collector area and storage volume: Other than the condensing temperature, also a proper combination of solar collector area as well as storage tank sizing is necessary to determine the reliability of the proposed system design. Figure 10 illustrates the combined effects of solar collector area and storage tank volume on its performance. It is evident from the trend that, initially an increase in storage volume effects a rapid rise in both COP and collector efficiency. However, for the storage tank volume beyond 150 liters, the performance parameters (COP and η_{coll}) do not improve much. On the other hand, for a given storage tank volume, an increase in solar collector area effects the system COP positively, though having a negative impact on the collector efficiency. This phenomenon could be attributed to two main reasons: (i) for a given solar collector area, increasing tank volume lowers the condensing temperature which eventually results only a marginal decrease in the solar collector/evaporator temperature. This paves a way for a relatively lesser amount of compressor work, in turn boosting the COP; (ii) For a given storage tank volume, an increase in solar collector area aids a rise in the fluid temperature of the evaporator, which results in an increase in COP, affecting a lower collector efficiency due to heat losses. Based on the numerical results, for the proposed DX-SAHP system, 100-150 liters m^{-2} turns out to be the optimum storage tank size.

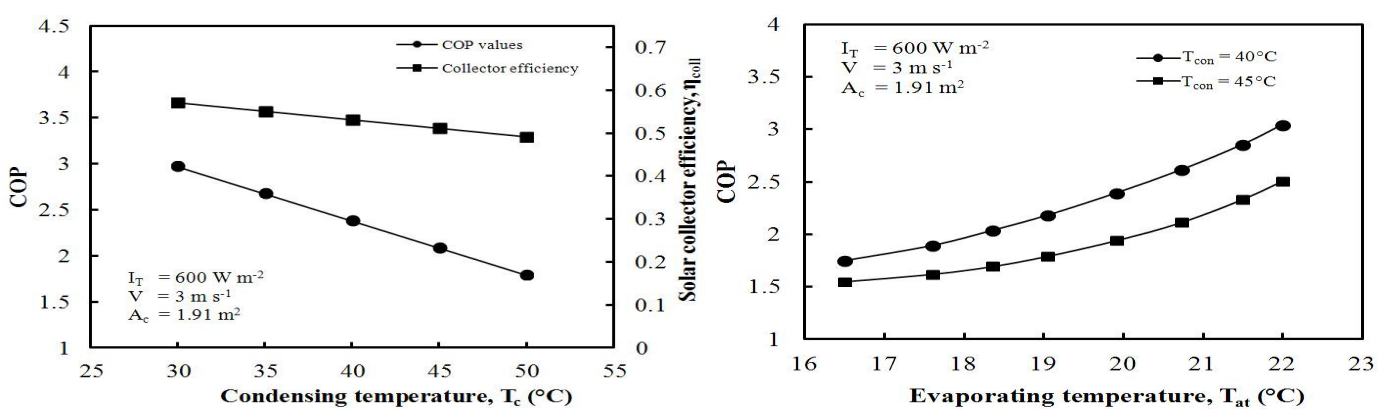

(a) (b)

Figure-9
Effect of (a) condensing temperature on system COP and collector efficiency; (b) evaporating temperature on COP at different condensing temperatures

Seasonal performance of the system: Long term seasonal performance of the heat pump system is normally computed by taking into account of the transient analysis for a given period of time interval. In the current study, the averaged monthly meteorological data of fall, winter and spring season of North Dakota, USA, have been utilized in simulations. Figure 11 shows the predicted variations in the performance factors, such as: the monthly averaged COP and solar collector efficiency. It is evident from the calculated results that COP of the system during winter months (about 3.0-3.2) is generally higher than the COP during fall and spring period (about 2.0-2.5). This is because, the difference between the condensation and evaporation temperature during winter months is particularly lower (figure 12). Lower temperature difference reflects less work requirement in the compressor which impacts an enhancement in the COP. In fall and spring, the system COP can be improved by lowering the compressor speed. Figure 11 also provides the monthly averaged collector efficiency variation (45%-62%), which confirms that the proposed system's collector efficiency is relatively higher compared to the conventional water driven solar flat-plate collector (~ 40%).

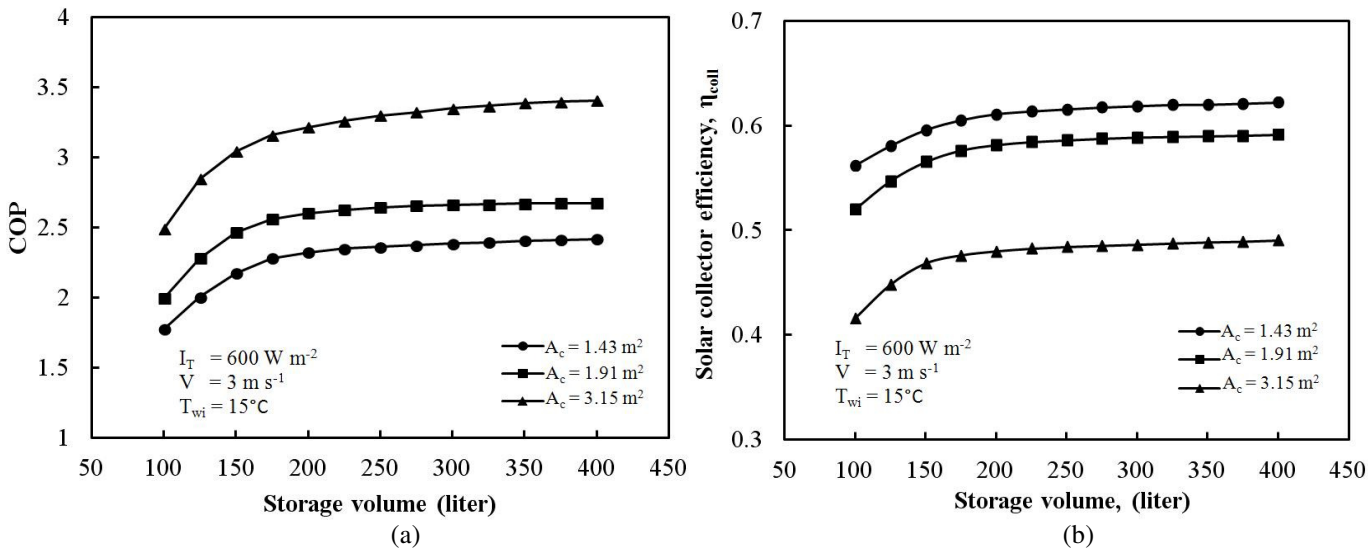

Figure-10
Combined effect of solar collector area and storage volume on the system performance: (a) COP values; (b) collector efficiencies

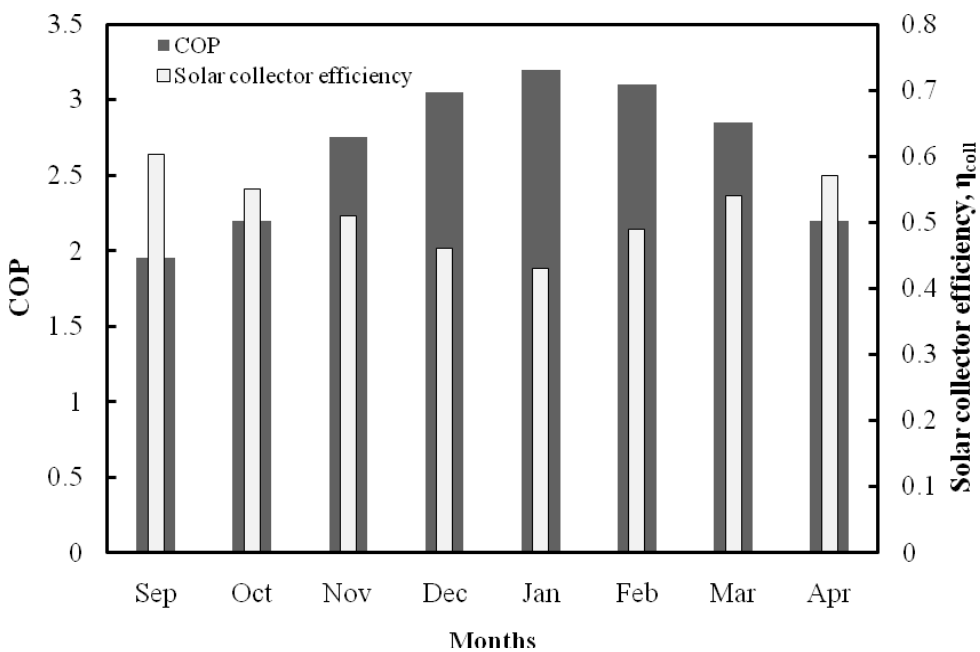

Figure-11
Variation of monthly averaged COP and solar collector efficiency in the fall, winter and spring season

Figure 12 illustrates the effect of seasonal variation on evaporator, condenser and water outlet temperature of the investigated model. For a given solar collector area and compressor speed, the difference between evaporator and condenser temperature in the fall and spring months remain higher compared to winter months. The larger temperature difference between T_{con} and T_f creates higher compressor work which negatively impacts the system COP.

Conclusion

A simulation model of direct expansion solar-assisted heat pump system has been studied using evacuated tube U-pipe solar collector and carbon dioxide as refrigerant for the water heating application. The parametric study along with seasonal variation of the heat pump system is discussed in this paper. Results have shown that, the thermal performance of the discussed system is greatly influenced by solar collector area, compressor speed, storage volume, evaporating and condensing temperature and the meteorological conditions. An optimum relation between the storage volume and solar collector area is found to be 100-150 liters m^{-2}. To ensure improved system performance, it is pertinent to choose an appropriate compressor speed which highly depends on the collector evaporative load. It is observed that average COP value increases by 57% when compressor speed decreases from 1500 to 900 rpm. The effect of seasonal variation on system performance analysis has shown that, the performance (COP) of the proposed heat pump system is much more pronounced during winter months, when usually the demand for hot water is high. Simulated results have shown that it is possible to achieve about 62% solar collector efficiency for an evacuated tube U-pipe collector, which is much higher than the conventional glass evacuated tube solar collector efficiency, using water as the working fluid (40-45%)[22]. Although the high initial cost of the evacuated tube U-pipe solar collector make the proposed DXSAHP water heating system to be expensive, the low cost and environmentally benign CO_2, has a great potential to be used in other integrated solar thermal applications as well.

Acknowledgement

This research was in part supported by a grant from the Pakistan-US Science and Technology Cooperation Program, US Department of State (jointly administered by the National Academics and Higher Education Commission of Pakistan).

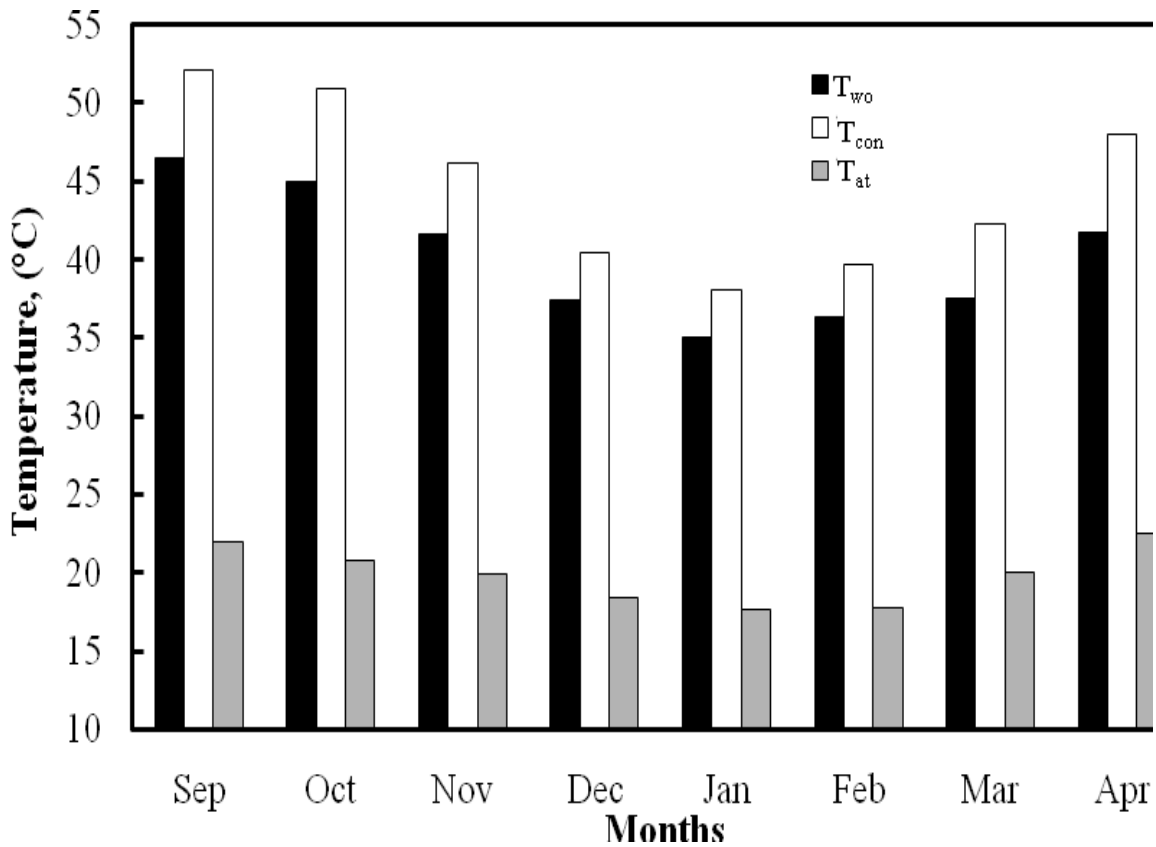

Figure-12
Variation of monthly averaged temperature profile for T_{wo}, T_{con}, and T_{at} in the fall, winter and spring months

Nomenclature: A area, (m^2), $A_{c,i}$ inner circular area of the condenser coil, (m^2) , $A_{c,o}$ outer circular area of the condenser coil, (m^2) , C_b bond conductance, (W m^{-1} K^{-1}), C_p specific heat capacity, (kJ kg^{-1} K^{-1}), C_{pv} average specific heat capacity at const. pressure and volume, (kJ kg^{-1} K^{-1}), C_f frictional pressure drop coefficient, COP coefficient of performance, D outer diameter, (m), d inner diameter of U-tube, (m), F fin efficiency, F' collector efficiency factor, f friction factor, G mass velocity, (kg $m^{-2}s^{-1}$), Gr Grashof number, g gravitational acceleration, (m s^{-2}), $h_{g,conv}$ convective heat transfer coefficient, (W m^{-2} K^{-1}), $h_{g,cond}$ conduction heat transfer coefficient, (W m^{-2} K^{-1}), $h_{g,r}$ radiation heat transfer coefficient, (W m^{-2} K^{-1}), h_{fg} enthalpy of vaporization, (kJ kg^{-1}), h enthalpy, (kJ kg^{-1}) / heat transfer coefficient, (W m^{-2} K^{-1}), h' heat transfer coefficient, (W m^{-2} K^{-1}), I_T global solar radiation intensity, (W m^{-2}), K thermal conductivity, (W m^{-1} K^{-1}), L length, (m), M mass, (kg), $\dot{m}$ mass flow rate, (kg s^{-1}), N compressor speed, (rpm), Nu Nusselt number, P pressure, (Pa) / electrical power inlet, (W), Pr Prandtl number, Q heat, (W), Q_u useful heat, (W), Q_{load} heat energy supplied to the load, (W), Re Reynolds number, Ra Rayleigh number, r radius, (m), S absorbed solar radiation, (W m^{-2}) / stroke length of comp, (m), T temperature, (°C), T_1 temperature at the outlet of solar collector, (°C), T_1' temperature of CO_2 in the collector at single-phase vapor region, (°C), ΔT degree of superheat, (°C), t simulated time, (s), U_L overall heat loss coefficient, (W m^{-2} K^{-1}), U_e edge loss coefficient, (W m^{-2} K^{-1}), U_t top loss coefficient, (W m^{-2} K^{-1}), UA overall heat transfer coefficient, (W m^{-2} K^{-1}), V wind speed, (m s^{-1}), V_s swept volume, (m^3), v = specific volume, (m^3 kg^{-1}), v_f specific volume of saturated liquid, (m^3 kg^{-1}), v_g = specific volume of saturated vapor, (m^3 kg^{-1}), v_{fg} change in specific volume, (m^3 kg^{-1}), W circumferential distance between U-tubes, (m), W_{com} = compressor work, (W), x= vapor quality, Z_0 = length at which refrigerant enters vapor region in evaporator (m)

Greek Letters: α = solar absorbtance, β = coefficient of thermal expansion, (K^{-1}), δ = thickness, (m), Δ = difference in quantity, λ = thermal conductivity, (W m^{-1} K^{-1}), ε = thermal emissivity, τ = solar transmittance, ρ = density, (kg/m^3), μ = dynamic viscosity, (N s m^{-2}), υ = kinematic viscosity, (N s m^{-2}), η = efficiency, σ = Stefan Boltzmann constant (5.67 x 10^{-8} W K^{-4} m^{-2})

Subscripts: A = ambience, At = absorber tube, B = bore, C = selective coating / CO_2, Con= condenser, $Coll$ = collector, $Coil$ = condenser coil, Dis = discharge, e =evaporator, f = fluid, g = glass/vapor, i = inlet, $isen$ = isentropic, m = metal/mechanical, o = outer, suc = suction, t = tank, v = vapor/volumetric, w = water.

References

1. The Kyoto Protocol to the United Nations Framework Convention on Climate Change, 1997. Accessed online: <http://untreaty.un.org/cod/avl/ha/kpccc/kpccc.html> **(2013)**
2. Freeman T. L., Mitchell J. W., Audit T. E., Performance of combined solar - heat pump systems, *Solar Energy*, **22(2)**, 125-35 **(1979)**
3. Macarthur J. W., Theoretical analysis of the dynamic interactions of vapor compression heat pumps, *Energy Conversion and Management*, **24(1),** 49-66 **(1984)**
4. Duffie J. A., Beckman W. A., Solar Engineering of Thermal Processes, second edition, Willey, New York, **(1991)**
5. Kaygusuz K., Gultekin N., Ayhan T., Solar-assisted heat pump and energy storage for domestic heating in Turkey, *Energy Conversion and Management*, **34(5)**, 335-46 **(1993)**
6. Axaopoulos P., Panagakis P., Kyritsis S., Experimental comparison of a solar-assisted heat pump vs. a conventional thermosyphon solar system, *International Journal of Energy Research*, **22(13)**, 1107-20 **(1998)**
7. Chaturvedi S. K., Abazeri M., Transient simulation of a capacity-modulated, direct-expansion, solar-assisted heat pump, *Solar Energy*, **39(5)**, 421-28 **(1987)**
8. Chaturvedi S. K., Chen D. T., Kheireddine A., Thermal performance of a variable capacity direct expansion solar-assisted heat pump, *Energy Conversion and Management*, **39(3-4)**, 181-91 **(1998)**
9. Hawlader M. N. A., Chou S. K., Ullah M. Z., The performance of a solar assisted heat pump water heating system, *Applied Thermal Engineering*, **21(10)**, 1049-65 **(2001)**
10. Huang B. J., Chyng J. P., Performance characteristics of integral type solar-assisted heat pump, *Solar Energy*, **71(6)**, 403-14 **(2001)**
11. Morrison G. L., Simulation of packaged solar heat-pump water heaters, *Solar Energy*, **53(3)**, 249-57 **(1994)**
12. Antoni M. D., Saro O., Massive Solar-Thermal Collectors: A critical literature review, *Renewable and Sustainable Energy Reviews*, **16(6)**, 3666-79 **(2012)**
13. Mills D., Advances in solar thermal electricity technology, *Solar Energy*, **76(1-3)**, 19-31 **(2004)**
14. Kalogirou S. A., Solar thermal collectors and applications, *Progress in Energy and Combustion science*, **30(3)**, 231-95 **(2004)**
15. Kim Y., Seo T., Thermal performances comparisons of the glass evacuated tube solar collectors with shapes of absorber tube, *Renewable Energy*, **32(5)**, 772-95 **(2007)**
16. Ma L., Lu Z., Zhang J., Liang R., Thermal performance analysis of the glass evacuated tube solar collector with U-tube, *Building and Environment*, **45(9)**, 1959-67 **(2010)**
17. Zhang X. R., Yamaguchi H., Uneno D., Fujima K., Enomoto M., Sawada N., Analysis of a novel solar energy-

powered Rankine cycle for combined power and heat generation using supercritical carbon dioxide, *Renewable Energy*, **31(12)**, 1839-54 **(2006)**

18. Zhang X. R., Yamaguchi H., Fujima K., Enomoto M., Sawada N., Study of solar energy powered transcritical cycle using supercritical carbon dioxide, *International Journal of Energy Research*, **30(14)**, 1117-29 **(2006)**

19. Yamaguchi H., Zhang X. R., Fujima K., Enomoto M., Sawada N., Solar energy powered Rankine cycle using supercritical CO_2, *Applied Thermal Engineering*, **26(17-18)**, 2345-54 **(2006)**

20. Yamaguchi H., Sawada N., Suzuki H., Ueda H., Zhang X. R., Preliminary study on a solar water heater using supercritical carbon dioxide as working fluid, *Journal of Solar Energy Engineering*, **132(011010)**, 1-6 **(2010)**

21. Zhang X. R., Yamaguchi H., Forced convection heat transfer of supercritical CO_2 in a horizontal circular tube, *Journal of Supercritical Fluids*, **41(3)**, 412-20 **(2007)**

22. Zhang X. R., Yamaguchi H., An experimental study on evacuated tube solar collector using supercritical CO_2, *Applied Thermal Engineering*, **28(10)**, 1225-33 **(2008)**

23. Kim M. H., Pettersen J., Bullard C. W., Fundamental process and system design issues in CO_2 vapor compression systems, *Progress in Energy Combustion Science*, **30(2)**, 119-74 **(2004)**

24. Lorentzen G., Trans-critical vapour compression cycle device. *International Patent Publication,* Patent No. WO 90/07683 **(1990)**

25. Lorentzen G., Pettersen J., A new, efficient and environmentally benign system for car air-conditioning, *International Journal of Refrigeration*, **16(1)**, 4-12 **(1993)**

26. Oritz T. M., Li D., Groll E. A., Evaluation of the performance potential of CO_2 as a refrigerant in air-to-air air conditioners and heat pumps: Systems modeling and analysis, *ARTI 2003*, Final report **(2003)**

27. Tamura T., Yakumaru Y., Nishiwaki F., Experimental study on automotive cooling and heating air conditioning system using CO_2 as a refrigerant, *International Journal of Refrigeration*, **28(8)**, 1302-07 **(2005)**

28. Kim M. H., Pettersen J., Bullard C. W., Fundamental process and system design issues in CO_2 vapor compression systems, *Progress in Energy Combustion Science*, **30(2)**, 119-74 **(2004)**

29. Kim S. G., Kim Y. J., Lee G., Kim M. S., The performance of a transcritical CO_2 cycle with an internal heat exchanger for hot water heating, *International Journal of Refrigeration*, **28(7)**, 1064-72 **(2005)**

30. Neksa P., Rekstad H., Zakeri G. R., Schiefloe P. A., CO_2-heat pump water heater: characteristics, system design and experimental results, *International Journal of Refrigeration*, **21(3)**, 172-79 **(1998)**

31. Neksa P., CO_2 heat pump systems, *International Journal of Refrigeration*, **25(4)**, 421-27 **(2002)**

32. Laipradit P., Tiansuwan J., Kiatsiriroat T., Aye L., Theoretical performance analysis of heat pump water heaters using carbon dioxide as refrigerant, *International Journal of Refrigeration*, **32(4)**, 356-66 **(2008)**

33. Cecchinato L., Corradi M., Fornasieri E., Zamboni L., Carbon dioxide as refrigerant for tap water heat pumps: A comparison with the traditional solution, *International Journal of Refrigeration*, **28(8)**, 1250-58 **(2005)**

34. Stene J., Residential CO_2 heat pump system for combined space heating and hot water heating, *International Journal of Refrigeration*, **28(8)**, 1259-65 **(2005)**

35. Richter M. R., Song S. M., Yin J. M., Kim M. H., Bullard C. W., Hrnjak P. S., Experimental results of transcritical CO_2 heat pump for residential application, *Energy*, **28(10)**, 1005-19 **(2003)**

36. Tian Q., Thermal performance of the U-type evacuated glass tubular solar collector, *Building Energy and Environment*, **26(3)**, 51-54 **(2007)**

37. Chaturvedi S. K., Chiang Y. F., Roberts A. S., Analysis of two-phase flow solar collectors with application to heat pumps, *Journal of Solar Energy Engineering*, **104(4)**, 358-65 **(1982)**

38. Oritz T. M., Li D., Groll E. A., Evaluation of the performance potential of CO_2 as a refrigerant in air-to-air air conditioners and heat pumps: System modeling and analysis, Final Report, *ARTI* , **(2003)**

39. Petukhov B. S., Heat transfer and friction in turbulent pipe flow with variable physical properties, *Advances in Heat Transfer*, **6**, 503-64 **(1970)**

40. Farrington R. B., Bingham C. E., Testing and analysis of load-side immersed heat exchangers for solar domestic hot water systems, *Technical Report (SERI/TR-254-3094)*, Solar Energy Research Inst., Golden, CO (USA) **(2013)**

41. North Dakota State Climate Office. North Dakota Annual Average Temperature. Accessed online: <http://www.ndsu.edu/ndsco/temp/monthly/2010.html> **(2013)**